

Published in final edited form as:

*Chem Biol.* 2011 February 25; 18(2): 252–263. doi:10.1016/j.chembiol.2010.12.008.

## Heterotaxin: a novel TGF- $\beta$ signaling inhibitor identified in a multi-phenotype profiling screen in *Xenopus* embryos

Michael K. Dush<sup>1</sup>, Andrew L. McIver<sup>2</sup>, Meredith A. Parr<sup>1</sup>, Douglas D. Young<sup>2</sup>, Julie Fisher<sup>3</sup>, Donna R. Newman<sup>1</sup>, Philip L. Sannes<sup>1</sup>, Marlene L. Hauck<sup>3</sup>, Alexander Deiters<sup>2,\*</sup>, and Nanette Nascone-Yoder<sup>1,</sup>

<sup>1</sup> Department of Molecular Biomedical Sciences, College of Veterinary Medicine, North Carolina State University, 4700 Hillsborough St., Raleigh, NC 27606

<sup>2</sup> Department of Chemistry, North Carolina State University, Raleigh, NC 27605-8204

<sup>3</sup> Department of Clinical Sciences, College of Veterinary Medicine, North Carolina State University, 4700 Hillsborough St., Raleigh, NC 27606

### Summary

Disruptions of anatomical left-right asymmetry result in life-threatening heterotaxic birth defects in vital organs. We performed a small molecule screen for left-right asymmetry phenotypes in *Xenopus* embryos and discovered a novel pyridine analog, heterotaxin, which disrupts both cardiovascular and digestive organ laterality and inhibits TGF- $\beta$ -dependent left-right asymmetric gene expression. Heterotaxin analogs also perturb vascular development, melanogenesis, cell migration and adhesion, and indirectly inhibit the phosphorylation of an intracellular mediator of TGF- $\beta$  signaling. This combined phenotypic profile identifies these compounds as a novel class of TGF- $\beta$  signaling inhibitors. Notably, heterotaxin analogs also possess highly desirable anti-tumor properties, inhibiting epithelial-mesenchymal transition, angiogenesis and tumor cell proliferation in mammalian systems. Our results suggest that assessing multiple organ, tissue, cellular and molecular parameters in a whole organism context is a valuable strategy for identifying the mechanism of action of novel compounds.

### Keywords

heterotaxia; TGF- $\beta$ ; Smad2; left-right asymmetry; *Xenopus*; pyridine

### Highlights

- 2,4,6-substituted pyridines disrupt left-right asymmetry in *Xenopus* embryos
- Pyridine compounds induce multiple TGF $\beta$ -dependent organ and cellular phenotypes

\*Contacts: Nanette Nascone-Yoder, Ph.D., Department of Molecular Biomedical Sciences, College of Veterinary Medicine, North Carolina State University, 4700 Hillsborough St., Raleigh, NC 27606, nanette\_nascone-yoder@ncsu.edu, P: 919-513-8284, F: 919-515-3044, Alexander Deiters, Ph.D., North Carolina State University, Department of Chemistry, Campus Box 8204, Raleigh, NC 27695-8204, alex\_deiters@ncsu.edu, P: 919-513-2958, F: 919-515-5079.

**Publisher's Disclaimer:** This is a PDF file of an unedited manuscript that has been accepted for publication. As a service to our customers we are providing this early version of the manuscript. The manuscript will undergo copyediting, typesetting, and review of the resulting proof before it is published in its final citable form. Please note that during the production process errors may be discovered which could affect the content, and all legal disclaimers that apply to the journal pertain.

- Pyridine compounds inhibit both Smad2- and non-Smad-dependent TGF $\beta$  signaling events
- Pyridine compounds inhibit EMT, angiogenesis and mammalian tumor cell proliferation

## Introduction

Vertebrate embryos develop with left-right asymmetry, evident in the asymmetric anatomical positioning of the heart and other vital organs. Correct asymmetries are essential for the function of the cardiovascular and digestive systems, and severe malformations are linked to disruptions of organ laterality. Complete reversal of normal left-right asymmetries (*situs inversus*) occurs in 1 in 8500 births (Brueckner, 2007), while “heterotaxia”, in which one or more organs deviate from normal by appearing independently and randomly oriented with respect to left and right, occurs in 1 in 10,000 births (Brueckner, 2007). Heterotaxia is often accompanied by intracardiac defects, and is associated with at least 3% of all congenital heart disease (Zhu et al., 2006). Also associated with heterotaxia is intestinal malrotation, which occurs in as many as 1 in 500 births and predisposes affected individuals to life-threatening conditions (Kamal, 2000).

The initial establishment of the left-right axis eventually results in the expression of genes exclusively on the left side of the embryo, including the TGF- $\beta$  family members *nodal* and *lefty*, and the transcription factor *Pitx2* (Levin, 2005). Although it has been demonstrated that *situs inversus* or heterotaxia can result if these genes are misexpressed, how such left-right cues are translated into the asymmetric morphology of developing organs is poorly understood. Such knowledge is essential for understanding the etiology of congenital deformities.

In recent years, whole-organism chemical genetic strategies, in which pharmacologically well-characterized small molecules are screened in living embryos for their ability to induce a developmental phenotype of interest, have been successfully used to illuminate the mechanisms which establish the initial left-right axis of the early embryo (e.g., Adams et al., 2006). However, the efficacy of such screening strategies is limited by the availability of known bioactives capable of exerting specific effects on developing model organisms. No discovery-based screens have been employed to uncover *novel* compounds that perturb left-right asymmetric organ morphogenesis. Identifying novel heterotaxia-inducing small molecules may not only offer an increased understanding of the molecular etiology of common birth defects, but may also reveal new classes of small molecules capable of modulating pathways that play important roles in development and disease.

Unfortunately, uncovering the mechanism of action of a novel molecule identified in a whole organism or phenotype-based screen remains a major challenge. Increasingly, multi-parameter phenotypic profiling is being used to categorize small molecules discovered in high-throughput biochemical assays or cell-based screens, providing insight into mechanism of action by similarities to reference compounds with known cellular targets (Feng et al., 2009). However, even compounds identified in multiplex strategies may still be ineffectual or have unpredictable or toxic effects *in vivo*.

Here we describe an approach to small molecule discovery that combines the advantages of whole organism screening and multiplex profiling by generating a multi-parameter profile of embryonic phenotypes. Recent studies have illustrated the promise of embryos of the aquatic frog, *Xenopus laevis*, for small molecule discovery (e.g., Tomlinson et al., 2009). A unique feature of *Xenopus* embryos, not found in other models (e.g., zebrafish), is the

morphogenesis of their left-right asymmetric organs, which is highly analogous to humans and easily visible *in situ* (Muller et al., 2003). We therefore employed *Xenopus* embryos in a screen for heterotaxia-inducing compounds, and identified a novel pyridine-based molecule, which we named “heterotaxin”. Further analyses of the *in vivo* phenotypic profile of this compound revealed that it elicits multiple TGF- $\beta$ -dependent phenotypes throughout development, and inhibits TGF- $\beta$ -dependent intracellular signaling events, identifying it as a new TGF- $\beta$  signaling inhibitor. Importantly, heterotaxin analogs also disrupt invasive phenotypes, angiogenesis and tumor cell proliferation in mammalian systems, revealing a new class of compounds with TGF- $\beta$ -inhibitory therapeutic potential.

## Results

### The discovery of heterotaxin (1)

A solid-supported multi-component cyclotrimerization reaction (Young et al., 2007) was utilized to generate a pilot library of ~130 novel natural product-like compounds as 44 pools of regioisomers. We arrayed *Xenopus laevis* embryos in individual wells of a 24-well plate in growth media supplemented with pools of regioisomers (200 $\mu$ M). After the embryos had completed asymmetric morphogenesis, the morphology of the heart and digestive tract was assessed in anesthetized tadpoles. All controls, i.e., untreated or exposed to DMSO alone, had normal organ asymmetries (Figure 1A, C–E, L), as did the embryos in 33/44 (75%) pools. In our initial screen, 2/44 pools (4.5%) were lethal at 200 $\mu$ M, and 8/44 pools (18%) elicited multiple defects (in organ, eye, craniofacial and tail development) in exposed embryos. However, one pyridine pool induced clear heterotaxia (heart and/or gut looping defects) in 100% of the exposed individuals (Figure 1B,F–K,M–N). In three repeat trials with embryos derived from oocytes obtained from different mothers, this pool was effective at inducing heterotaxia in at least 50% of embryos exposed at a concentration of 100–200 $\mu$ M. Overall, 89% (n=28) of the embryos in all trials that were exposed to the active regioisomer pool at 100–200 $\mu$ M exhibited heterotaxia phenotypes, strongly implicating one or more regioisomers in this pool as an inhibitor of a cellular target(s) required for normal left-right asymmetric organ development.

### Identification of the active heterotaxia-inducing regioisomer

To facilitate the isolation of the regioisomer responsible for the observed heterotaxia phenotypes, the solid-phase synthesis used to generate the original pool was conducted on a five-fold larger scale. A GC trace of the heterotaxia-inducing pool prior to purification indicated the presence of several different regioisomers (Figure 2A). After separating these components by flash-column chromatography on silica-gel, we found that only the 2,4,6-regioisomer **1** (Figure 2B; GC retention time of 17.17min) displayed the ability to induce the desired phenotype in *Xenopus* embryos (not shown).

As further confirmation, we exposed embryos of a related species, *Xenopus tropicalis*, to this purified component. Despite the differences between the *X. laevis* and *X. tropicalis* species in culture temperature (15°C vs. 24°C, respectively), size (1.2mm vs. 0.7mm, respectively) and growth rate (7–8 days vs. 3–4 days, respectively), the regioisomerically pure compound induced identical heterotaxic organ deformities in both the heart and gut as observed in *X. laevis* (data not shown). Due to its “heterotaxia-inducing” propensity, we named the purified, active regioisomer “heterotaxin.”

### A regioselective synthetic route to heterotaxin

Our original synthesis route towards heterotaxin necessitated laborious purification of the 2,4,6-regioisomer **1** from a mixed pool and was therefore inefficient for generating the large (gram) quantities of heterotaxin required for further characterization. Consequently, we

developed a robust, scalable synthetic approach to heterotaxin, with a sequence of chemical transformations that provided a completely regioselective synthesis (Figure 2C).

The synthesis commenced with the condensation of the lithiated trityl protected propargyl alcohol **2** and commercially available chlorodiisopropylsilane (**3**) to afford the silane **4** in 76% yield.<sup>1</sup> The silane **4** was then subjected to *in situ* bromination by NBS followed by a subsequent reaction with propargyl alcohol in the presence of TEA and DMAP in DCM to afford the silyl ether **5** in 85% over two steps.<sup>1</sup> The key step of the synthesis was a microwave-mediated, cobalt-catalyzed [2+2+2] cyclotrimerization reaction between the diyne **5** and propionitrile under open-vessel conditions. This delivered the pyridine **6** in 98% yield. The silicon tether allowed for a completely regio-selective pyridine formation (Bols and Skrydstrup, 1995), with the C-N bond being formed with the substituted *sp*-carbon center bearing the CH<sub>2</sub>OTrt group. The silicon tether was then removed using TBAF in refluxing THF to afford the regioisomerically pure 2,4,6-substituted pyridine **9** in 99% yield. The alcohol **9** was converted into the aldehyde **12** in 90% yield using a Swern oxidation. Following the oxidation, a Wittig reaction was employed to install the C<sub>4</sub> chain at the 4-position affording the alkene **15** in a moderate yield of 78%. Reduction of the double bond in **15** with Pd/C under 1 atm of H<sub>2</sub> furnished the pyridine **21** in almost quantitative yield. The acid-catalyzed deprotection of the trityl group proceeded smoothly and delivered heterotaxin (**1**) in 100% yield. This schematic route allowed us to synthesize reasonable (37 mg) quantities of heterotaxin, and analogs thereof (see below), which we used to further investigate the mechanism by which it induces heterotaxia, and to elucidate its mechanism of action.

### Multiple phenotypes are induced by heterotaxin

Heterotaxin perturbs organ laterality, suggesting that it interferes with global embryonic left-right patterning. Indeed, heterotaxin perturbs left-right asymmetric gene expression patterns in the lateral plate mesoderm (LPM). For example, in heterotaxin-treated embryos, the pattern of the *Xenopus nodal* homologue, *Xnr-1*, is randomized with respect to left and right (Figure 3A–D). While some embryos exhibit normal left side *nodal* expression (36%, n=28), some show bilateral *nodal* expression on both the left and right sides (18%, n=28), some exhibit reversed (i.e., right-sided) *nodal* expression (11%, n=28) and some (36%, n=28) completely lack *nodal* expression on either side (Figure 3I). As expected, the expression patterns of the *Xenopus* homologue of *Pitx2*, a transcription factor whose expression is dependent on *nodal* activity, is similarly randomized by exposure to heterotaxin (Figure 3E–H, J). These results confirm that the organ anomalies induced by heterotaxin represent *bona fide* left-right asymmetry defects.

To gain further information about heterotaxin's mechanism of action, we carefully assessed heterotaxin-treated embryos throughout development (Figure 4). Compared to DMSO-treated controls (Figure 4A), the melanocytes in heterotaxin-treated tadpoles exhibit a striking increase in pigmentation and dendricity (Figure 4B–C), and the number of melanocytes is reduced by as much as 50% (Figure 4D). Exposure to heterotaxin also results in dilated vitelline vessels and ventral hemorrhaging (Figure 4E–G), suggesting that the compound perturbs the normal processes of vasculogenesis and/or angiogenesis.

Finally, in addition to being malrotated, the digestive tracts of embryos exposed to heterotaxin are wider and shorter than controls (e.g., see Figure 4E, G). The elongation of the digestive tract is driven by the rearrangements of endoderm cells within the embryonic gut tube, a process which also facilitates the formation of the gut lumen and epithelial lining (Reed et al., 2009). The endoderm cells are initially round, but adopt an elongated shape and remodel their intercellular adhesive junctions as they move toward the circumference of the gut, intercalating between each other to form a single layer (Reed et al., 2009). In controls,

the resultant simple columnar epithelium can be observed lining the lumen of the lengthened coils of gut (arrows, Figure 4H). In contrast, in heterotaxin-treated embryos, the digestive epithelium is still stratified and contains clumps of rounded cells that have failed to rearrange into a single layer (arrows, Figure 4I–J). These dysmorphic cells block the gut lumen and exhibit increased intercellular adhesion, as indicated by their intensified E-cadherin staining (arrows and insets, Figure 4I–J). This unusual morphology suggests that the normal acquisition or maintenance of migratory cell properties in the embryonic endoderm is inhibited in these embryos, preventing the cell rearrangements required for normal gut elongation.

### Identifying the phenocritical period for the effects of heterotaxin

To determine the phenocritical period in which heterotaxin elicits each of the above phenotypes, we exposed embryos to heterotaxin for limited times (Figure 4K). The expression of left-right genes in the *Xenopus* embryo peaks between stages 19 and 26 (Ohi and Wright, 2007). To determine whether heterotaxin directly affects left-right gene expression or function, we exposed embryos to heterotaxin at successively later stages of development beginning at stage 12 (gastrula), 18 (neurula), 26 (late neurula), or 32 (tailbud). The compound can elicit robust heterotaxic organ phenotypes when applied as late as stage 18, but will induce heterotaxia only at low frequency at stage 26, and has no effect on organ asymmetry when applied at stage 32 (Figure 4K). We then exposed embryos to heterotaxin through stage 26, washed away the compound with multiple rinses in fresh media, and cultured in the absence of heterotaxin through organogenesis. We found that even this limited exposure can disrupt organ asymmetries (Figure 4K), suggesting that heterotaxin affects left-right asymmetry between stages 18 and 26, coinciding with the peak of left-right gene expression.

We used similar exposures to determine the period in which heterotaxin induces other phenotypes. The melanogenesis phenotype can be elicited even when heterotaxin is applied as late as stage 32 (Figure 4K), suggesting that the compound acts directly on developing melanocyte precursors, which migrate and differentiate between stage 30 and 40 (Collazo et al., 1993). Likewise, the effect on gut elongation can also be elicited by exposure to the compound as late as stage 32 (Figure 4K), just prior to when migratory properties are acquired by endoderm cells in the embryonic gut (Reed et al., 2009), indicating that heterotaxin exerts a direct effect on these cells. In contrast, the frequency of heterotaxin-induced vasculogenesis/angiogenesis defects declines at stage 32 (Figure 4K). Since the genes that regulate the formation of the vitelline veins are expressed between stage 18 and 28 (Walmsley et al., 2002), and the vascular vitelline network is already forming at stage 30 (Inui and Asashima, 2006), the observed window of susceptibility to heterotaxin is consistent with the timing of neovascularization. Overall, these results suggest that multiple independent phenotypes in heterologous tissues result from heterotaxin acting directly and specifically on discrete populations of embryonic cells at different stages of development.

### Structure activity relationship (SAR) studies of heterotaxin

To further explore heterotaxin's multifunctionality, we conducted structure-activity relationship studies with heterotaxin analogs. Our regioselective route to heterotaxin (Figure 2), was purposely designed in a flexible fashion to enable the introduction of other substituents on the pyridine ring through the selective replacement of the butyl and the ethyl side chain with additional functional groups. This enabled the assembly of a small set of analogs from a common intermediate. The R<sup>1</sup> and R<sup>2</sup> groups were selected as methyl, ethyl, propyl, phenyl, and hydroxymethylene, based on the original side chains found in heterotaxin and in order to probe the size of the putative cellular protein binding pocket. Thus, we synthesized substantial quantities of the diyne **5**, and used that to branch out to the

synthesis of analogs. The key step was again a cobalt-catalyzed [2+2+2] cyclotrimerization reaction between the diyne **5** and a variety of different nitriles (propionitrile, valeronitrile, and benzonitrile), delivering the fused, regioisomerically pure pyridines **6–8** ( $R^1$  = ethyl, butyl, phenyl) in 82–98% yield. The silicon tether was then removed using TBAF to afford the 2,4,6-substituted pyridines **9–11** in 86–99% yield. The alcohols **9–11** were converted into the aldehydes **12–14** in 84–90% yield using the previously employed Swern oxidation, followed by a Wittig reaction with several different alkylphosphonium bromides to install different chain lengths at the 4-position in **15–20** ( $R^2$  = methyl, propyl, butyl, pentyl). Reduction of the double bond in **15–20** with Pd/C under 1 atm of  $H_2$  furnished the pyridines **21–26** in almost quantitative yields. The acid-catalyzed deprotection of the trityl group proceeded smoothly and delivered the heterotaxin analogs **27–31** in 71–100% yield.

Two additional analogs were synthesized by deprotection of the trityl group at different stages of the synthesis (Figure 5). One deprotection was conducted after removal of the silicon tether from **9** to afford the diol **32** in 66% yield, and the second was performed on the alkene **16** to obtain the compound **33** in 63% yield. Installation of different hydrocarbon substituents on the hydroxyl group of heterotaxin (**1**) was accomplished by subjecting **1** to deprotonation with NaH followed by the addition of the appropriate alkyl halide (methyl, benzyl, and hexyl) to afford the ethers **34–36** in 42–86% yield. Finally, the hydroxyl group of heterotaxin (**1**) was oxidized to the carboxylic acid **38** by a two-step oxidation process. First, the aldehyde **37** was formed in moderate yield by oxidation of the alcohol **1** with  $MnO_2$ , followed by a Lindgren oxidation<sup>3, 4</sup> to form the carboxylic acid **38** in 89% yield (Figure 5).

The length of the alkyl chain at the  $CH_2R^2$  substituent was found to be critical for the specific activity of this class of molecules, with the highest activity being observed for butyl (heterotaxin, **1**) and pentyl (**28**), while ethyl (**27**), ethylene (**33**), hydroxymethylene (**32**), and hexyl (**29**) were inactive (or toxic; Table S1). Although the size of the  $R^1$  group does not appear to be critical, as ethyl (heterotaxin, **1**), butyl (**31**), and phenyl (**30**) are tolerated, both the butyl (**31**) and phenyl (**30**) substitutions did yield more potent analogs, which exhibited activity at lower concentrations than the original heterotaxin molecule ( $EC_{50}$  values = 10 and 50  $\mu M$ , respectively; Table S1). Furthermore, although modifications of the  $CH_2OH$  group through methylation (**34**), oxidation (**38**) or alkylation (**36**) did not have a major effect on activity, benzylation (**35**) produced a very active compound ( $EC_{50}$  value = 10  $\mu M$ ; Table S1). Interestingly, for each analog, the  $EC_{50}$  for inducing defects in asymmetric organogenesis was identical to the  $EC_{50}$  for perturbing melanogenesis, vasculogenesis/angiogenesis, and/or gut elongation, although the severity of each phenotype varied between analogs (see Table S1). These results show that replacing individual substituents does not isolate the various activities of the compound, suggesting that the individual phenotypes induced by heterotaxin are not chemically separable and may result from perturbation of the same biological target.

### Identifying the cellular target of heterotaxin analogs

Our phenocritical timing studies suggest that heterotaxin perturbs left-right asymmetry during the stages when asymmetrically-expressed TGF- $\beta$  ligands, such as *nodal*, establish organ laterality. Therefore, we hypothesized that TGF- $\beta$  signaling is inhibited by heterotaxin. Because the above SAR studies indicate that the various phenotypes induced by heterotaxin are not chemically separable, it is possible that the complete phenotypic profile of this compound is attributable to inhibited TGF- $\beta$  signaling. This hypothesis is strongly supported by the fact that exposure to a known small molecule TGF- $\beta$  signaling inhibitor, SB505124 (DaCosta et al., 2004), induced the same phenotypic profile as our compounds, including heterotaxia, vasculogenesis and melanogenesis defects, and aberrant migratory cell properties, within the same phenocritical periods (Figure S1). Importantly, other

signaling pathways that also influence all four of these developmental processes are unaffected by heterotaxin (Figure S1).

To test the hypothesis that heterotaxin interferes with TGF- $\beta$  signaling, we evaluated the expression of *Xantivin*, the *Xenopus* homologue of *lefty*, which is normally expressed in the left LPM as a direct consequence of *nodal*-type TGF- $\beta$  signaling (Ho et al., 2006). Although DMSO-treated control embryos exhibit normal expression of this target gene in the left LPM, *Xantivin* could not be detected in the left or right LPM of heterotaxin-treated embryos (Figure 6A and Figure S2), strongly suggesting that *nodal*-type TGF- $\beta$  signaling is inhibited by heterotaxin. These data are consistent with previous reports in which embryos exposed to a known TGF- $\beta$  signaling inhibitor failed to express *Xantivin* (Ho et al., 2006).

TGF- $\beta$  receptor activation is conveyed by the phosphorylation of intracellular mediators, known as Smads, which ultimately effect transcription (ten Dijke and Hill, 2004). *Nodal* signaling occurs primarily via phosphorylation of Smad2; thus, the level of phosphorylated Smad2 in *Xenopus* extracts may be used as an indicator of embryonic *nodal*-type TGF- $\beta$  signaling (Ho et al., 2006). As expected, the level of phosphorylated Smad2 is unaffected by exposure to DMSO (Figure 6B, lane 1). However, Smad2 phosphorylation is abolished in embryos exposed to heterotaxin (**1**; Figure 6B, lane 2), or to the more potent heterotaxin analog **35** (Figure 6B, lane 4), but is only mildly downregulated by exposure to the phenotypically inactive heterotaxin analog **32** (Figure 6B, lane 3). The inhibition of Smad2 phosphorylation by heterotaxin is comparable to that induced by SB-505124 (Figure 6B, lane 5). Importantly, the level of phosphorylated Smad1/5/8, which indicates signaling via other TGF- $\beta$  superfamily ligands such as BMP, remains unaffected by heterotaxin analogs (Figure 6B); thus, the effect of heterotaxin is specific for Smad2-dependent TGF- $\beta$  signaling.

A unique advantage of amphibian embryos is the ability to culture specific embryonic tissues *ex vivo* in order to isolate the effects of exogenous growth factors on cell behavior. It is well-established that the addition of the Smad2-mediated TGF- $\beta$  ligand activin to *Xenopus* “animal cap” explants can elicit concentration-dependent elongation in a tissue that would otherwise remain naïve to TGF- $\beta$  signals and fail to elongate at all (Green, 1999). We employed this assay to quantify the degree to which heterotaxin analogs interfere with TGF- $\beta$ -ligand-dependent signaling. In contrast to DMSO or the inactive analog **32**, heterotaxin (**1**) and the potent analog **35** significantly inhibit activin-induced animal cap elongation, (Figure 6D); thus, heterotaxin analogs inhibit activin-dependent activity in *Xenopus*.

To determine if heterotaxin analogs inhibit the activity of other TGF- $\beta$  ligands, we assessed their activity in human cell culture. A549 cells undergo an epithelial-mesenchymal transition in response to TGF- $\beta$ 1 (Kim et al., 2007), as indicated by the upregulation of mesenchymal markers such as Snail and Vimentin (Figure 6E, compare lanes 1–2). Heterotaxin (**1**) and the potent analog **35** inhibit the upregulation of these markers, (Figure 6E, lanes 4–7), while DMSO or the inactive analog **32** have no effect (Figure 6E, lanes 3, 8–9); thus, heterotaxin analogs inhibit TGF- $\beta$ 1-dependent activity in human cells.

To determine if heterotaxin compounds directly affect ligand-dependent Smad2 phosphorylation, we assessed levels of phosphorylated Smad2 in these cells with a one-hour TGF- $\beta$ 1 induction (Figure 6F). Compared to the effect of SB431542, a known TGF- $\beta$  Type I receptor inhibitor (Inman et al., 2002), TGF- $\beta$ 1-induced Smad2 phosphorylation remained relatively unaffected by our compounds in this time frame, suggesting that the effect of heterotaxin on Smad2 phosphorylation *in vivo* may not involve direct inhibition of TGF- $\beta$  receptors or may inhibit a non-smad-dependent TGF- $\beta$  signaling pathway (Zhang, 2009).

We tested the latter possibility by assessing the effect of heterotaxin on TGF- $\beta$ -induced activation of phosphatidylinositol-3-kinase (PI3K), as well as mitogen-activated protein kinases (MAPKs), including p38, c-Jun amino-terminal kinase (JNK), and extracellular signal-regulated kinase (ERK). Although the activation of most of these non-Smad pathways was not suppressed by our compound (data not shown), TGF- $\beta$ -induced activation of PI3K (1 hour induction), as indicated by the levels of phosphorylated Akt (Ser-473; Figure S2E, lanes 1–2), was inhibited by heterotaxin (**1**; Fig S2E, lanes 4–5), while DMSO and the inactive analog **32** had no effect (Figure S2E, lanes 3, 6). Taken together, these results indicate that 2,4,6-substituted pyridines function as both indirect (Smad2-dependent) and direct (non-Smad-dependent) TGF- $\beta$  signaling inhibitors.

### Heterotaxin analogs exhibit anti-angiogenic properties in mammalian cells

In addition to development, the TGF- $\beta$  pathway also plays a multiphasic role in tumor progression. Although early in tumorigenesis TGF- $\beta$  is tumor suppressive (Jakowlew, 2006), later tumor cells are resistant to TGF- $\beta$ -mediated growth inhibition, and upregulation of TGF- $\beta$  facilitates metastatic invasion, promoting cell migration and epithelial-to-mesenchymal transition (Yingling et al., 2004; Tian et al., 2003), as well as new blood vessel growth and angiogenesis (ten Dijke and Arthur, 2007), crucial requirements for tumor growth and metastasis.

TGF- $\beta$  signaling inhibitors, like heterotaxin and its analogs, may therefore be useful for blocking the tumor-promoting effects of TGF- $\beta$ . Since our compounds inhibit vascular development *in vivo*, we assessed their anti-angiogenic potential in a mammalian system (Figure 7). The human umbilical vein endothelial cell (HUVEC) assay provides a visual readout of the ability of exogenous factors to inhibit the formation of microcapillary tubes (e.g., Figure 7D). Compared to solvent or pyridine controls (Figure 7B–C), the heterotaxin analogs that inhibited vascular development in *Xenopus* (e.g., **1**, **30**, **35**, **36**; see Table S1) were also able to inhibit tube formation (Figure 7F–I) in HUVEC cultures. The effects were comparable to those elicited by a known TGF- $\beta$  receptor inhibitor (Figure 7E). However, while TGF- $\beta$  receptor inhibitors can also block the growth-inhibitory effects of TGF- $\beta$  (e.g., SB-431542; Halder et al., 2005), promoting tumorigenesis, heterotaxin analogs appear not to have this limitation. In fact, compound **30** not only inhibits angiogenesis (Figure 7I), but significantly inhibits growth in several mammalian tumor cell lines (Figure S3). Thus, 2,4,6-substituted pyridine analogs may be broadly applicable in the development of anti-angiogenic anti-tumor compounds in mammalian systems.

## Discussion

A multi-phenotype-based whole organism screen of small molecules in *Xenopus laevis* embryos identified a novel class of pyridines with TGF- $\beta$  inhibitory activity. Our data have implications for understanding the role of the TGF- $\beta$  pathway in the development of left-right asymmetry, gut morphogenesis, melanogenesis and vascular development, and for the employment of heterotaxin analogs in the development of TGF- $\beta$  inhibitory lead compounds with therapeutic potential.

### Heterotaxin and the role of TGF- $\beta$ in left-right asymmetry, melanogenesis, vasculogenesis and gut development

Our results validate our phenotypic screen for heterotaxia because TGF- $\beta$  ligands are well known to play an evolutionarily conserved role in the development of left-right asymmetry (Whitman and Mercola, 2001). Moreover, in addition to left-right patterning, TGF- $\beta$  signaling has also been implicated in the other biological processes disrupted by heterotaxin. For example, TGF- $\beta$  signaling is required for the assembly of the embryonic vasculature



(ten Dijke and Arthur, 2007), the establishment of vessel wall integrity (Pepper, 1997), and the regulation of vascular homeostasis (Bertolino et al., 2005). As might be predicted to occur in the presence of a TGF- $\beta$  inhibitor, heterotaxin dramatically impairs angiogenesis both *in vivo* and *in vitro*. Because *in vitro* tube formation may also be influenced by other factors, confirmation of a direct effect of heterotaxin on human angiogenesis must await further studies in mammalian models. Nonetheless, the similarity of the anti-angiogenic activity profiles of heterotaxin analogs in both frog embryos and human cells suggests that these compounds could have broader applicability.

In addition, TGF- $\beta$  signaling normally increases melanocyte precursor proliferation (Kawakami et al., 2002), but inhibits melanogenic differentiation (Kim et al., 2004). Consistent with the expected outcome of inhibiting TGF- $\beta$  signaling, heterotaxin exposure during melanocyte precursor migration and differentiation results in decreased melanocyte number but increased dendricity. As *nodal* is expressed in aggressive melanomas, which re-acquire melanocyte precursor-like properties, heterotaxin analogs may be promising in the development of differentiation-based anti-melanoma therapies (Hendrix et al., 2007).

Finally, in multiple contexts, TGF- $\beta$  signaling induces cell motility and decreased E-cadherin-mediated intercellular adhesion in cells undergoing epithelial-to-mesenchymal transitions (Xu et al., 2009). In the developing gut, heterotaxin inhibits migratory cell morphology and behavior, and concomitantly increases E-cadherin levels, as might be predicted for an inhibitor of TGF- $\beta$  signaling. The effect of heterotaxin on gut morphogenesis provides a novel inroad for investigating the role of TGF- $\beta$  signaling in the poorly understood processes of gut elongation and rotation.

### The cellular target of heterotaxin

Heterotaxin compounds disrupt Smad2 phosphorylation *in vivo*, although this is not a direct effect. Possible mechanisms of action of heterotaxin and its analogs include inhibiting the synthesis, secretion or processing of TGF- $\beta$  receptors or ligands. Alternatively, these compounds could be influencing non-Smad-dependent pathways downstream of TGF- $\beta$  receptors. Indeed, we found that Heterotaxin directly inhibits TGF- $\beta$ -induced phosphatidylinositol-3-kinase (PI3K) activity. Although activation of PI3K by TGF- $\beta$  requires the activity of TGF- $\beta$  receptors, the molecular interactions underlying the activation of non-smad-dependent TGF- $\beta$  signaling events are extremely complex and context-dependent (Zhang, 2009). Therefore, further investigations of the role of PI3K-mediated TGF- $\beta$  signaling during *Xenopus* development will be required before the cellular target(s) of 2,4,6-substituted pyridines can be fully resolved. Nonetheless, because non-Smad-dependent TGF- $\beta$  pathways are frequently involved in activating the pro-oncogenic effects of TGF- $\beta$  signaling during tumor progression—e.g., PI3K-Akt signaling is required for Smad-dependent transcriptional responses as well as tumor cell migration (Bakin et al., 2000)—our results raise the exciting possibility that heterotaxin compounds might be able to selectively target TGF- $\beta$ -dependent tumor-promoting outcomes without also blocking the tumor-suppressive effects of TGF- $\beta$ . This property could be important for selectively controlling distinct TGF- $\beta$  responses in different therapeutic contexts.

### Heterotaxin analogs as therapeutic agents

Because of their important roles in tumorigenesis, TGF- $\beta$  pathway components are excellent chemotherapeutic targets, although compounds that can appropriately modulate this multifunctional pathway *in vivo* are still in development. We discovered compounds that specifically inhibit *nodal*-dependent gene expression and multiple TGF- $\beta$ -dependent biological processes in a whole vertebrate embryo, including neovascularization and migratory behavior. In addition, heterotaxin analogs inhibit TGF- $\beta$ -induced epithelial-

mesenchymal transition and angiogenesis in human cells, while inhibiting the growth of multiple mammalian tumor cell lines. Thus, heterotaxin analogs exhibit highly desirable biological activity and may be valuable in the development of TGF- $\beta$ -inhibitory chemotherapeutics for blocking tumor proliferation and/or metastasis.

## Significance

In the developing embryo, a myriad of cellular processes form organs in a dynamic and complex three-dimensional milieu. In disease states, these same processes occur inappropriately in equally complicated adult environments. Identifying small molecules that can predictably modulate cellular processes in their multifarious biological contexts is imperative for the discovery of effective drugs and stem cell therapies. However, many lead compounds are initially identified in target-based biochemical or simplified cell-based assays because such assays are amenable to high throughput screening; consequently, the *in vivo* effects of such compounds are often unpredictable. While multiplexed profiling can provide important information about potential toxicity and mechanism of action, such knowledge is not necessarily predictive of efficacy *in vivo*. Moreover, even when a novel compound has been identified in a whole organism phenotype-based screen, there is as yet no reliable or systematic way to determine its cellular target(s).

We have shown that a whole-organism multi-phenotype profiling strategy can be used to both identify novel compounds capable of modulating important biological processes *in vivo*, and to infer mechanism of action. Using a combination of independent tissue-level developmental phenotypes, immunohistochemical analyses, gene expression patterns, tissue culture and biochemical assays, we discovered a novel class of TGF- $\beta$  signaling inhibitors. Remarkably, these compounds also elicit TGF- $\beta$ -dependent phenotypes in human cells that mirror their activity profiles *in vivo*, suggesting that they may be valuable in the development of therapeutic agents to inhibit pathologic conditions mediated by excess TGF- $\beta$  signaling (e.g., metastasis, fibrosis). Our discovery suggests that multi-phenotype profiling in whole organisms is a powerful strategy for identifying the pathway-level mechanism of action of novel small molecules.

## Experimental Procedures

### Embryo screening and animal caps

Experiments involving live animals were performed in accordance with national regulations, and approved by the NC State University Institutional Animal Care and Use Committee. *Xenopus laevis* embryos were obtained by *in vitro* fertilization, de-jellied with 2% cysteine-HCl pH 7.8–8.1, sorted to eliminate anomalous individuals and cultured in 0.1X MMR at 15°–22°C (Sive et al., 1998). Staging was according to Nieuwkoop and Faber (1994).

Stock solutions were prepared in DMSO (20mM). For the screen, approximately ~130 compounds were diluted to 200 $\mu$ M in 2 mls 0.1X MMR in a 24-well plate; 1% DMSO was used as a solvent control. Four embryos were exposed in each well starting at ~10 hrs post fertilization. Organs were evaluated in anesthetized tadpoles (0.05% MS-222) when controls reached stage 44–46.

Animal caps were dissected (Green, 1999), and cultured in 5 ng/ml human activin A (R&D Systems), or activin plus DMSO, 200 $\mu$ M **1**, **32**, or **35** for 2 hrs. Caps were then cultured 8 hrs in 0.75X MMR + gentamycin (Sive et al., 1998). Final explant lengths were calculated using Photoshop CS2 (Measure tool). The significance of decreased elongation was determined by one-way ANOVA between groups.

### ***In situ* hybridization and immunohistochemistry**

Embryos were fixed at st 23/26 in MEMFA (Sive et al., 1998). Digoxigenin-labeled riboprobes for *Xnr-1*, *XAntivin* (gift of C. Wright), and *XPitx2c*, were synthesized from linearized plasmids (Muller et al., 2003). *In situ* hybridization was as described (Lipscomb et al., 2006). St 44 embryos were fixed for immunohistochemistry and processed for cryosectioning (Fagotto and Gumbiner, 1994). Staining was performed using anti-E-cadherin (DSHB, 5D3 at 1:200) and anti-laminin (Sigma, L9393 at 1:200) primary antibodies and Alexa-conjugated secondary antibodies (Invitrogen, 1:2000), as described (Reed et al., 2009).

### **Tube formation**

HUVEC cells were cultured in Media 200PRF with LSGS supplement (Invitrogen). The Cultrex<sup>®</sup> In Vitro Angiogenesis Assay Tube Formation Kit (Trevigen) was used according to manufacturer's protocol. Subconfluent HUVECs at passage 5 (~80% confluent) were incubated with 2 $\mu$ M Calcein AM for 30 min at 37°C to allow for fluorescent monitoring of cell viability and tube formation. Cells were treated with DMSO, sulforaphane, or heterotaxin analogs/SB-505124 at the time of seeding. Tube formation was assessed 6 hrs after treatment.

### **Western blotting**

St 10 embryos were exposed to DMSO, heterotaxin analogs, SB-505124, or Dorsomorphin for 24 hrs. Ten embryos from each treatment were pelleted, resuspended in 100 $\mu$ l lysis buffer (20mM Tris pH7.4, 150mM NaCl, 1mM EDTA, 1mM EGTA, 1% Triton, 2.5mM sodium pyrophosphate, 1mM b-glycerophosphate, 1mM sodium vanadate, 1 $\mu$ g/ml leupeptin) and lysed by mechanical disruption, followed by freeze-thaw cycles. Approximately 20 $\mu$ g of each cleared lysate was run on a 10% NuPAGE Bis-Tris gel and then transferred to a PVDF membrane. Membranes were blocked for 1 hr in TBST (20mM Tris pH 7.6, 136mM NaCl, 0.1% Tween-20) + 5% non-fat dry milk, and incubated overnight at 4°C with primary antibodies (see below). Membranes were washed 4 times in TBST, incubated for 2 hrs in TBST+ 5% non-fat dry milk and HRP-conjugated donkey anti-rabbit IgG (Upstate), washed 3–4 times in TBST, then visualized using chemiluminescence with SuperSignal West Pico (Pierce).

A549 cells (ATCC) were maintained in DMEM with antibiotics and 10% FBS. Cells were starved overnight in DMEM with 1% FBS and incubated with DMSO, heterotaxin analogs or SB-431542 in DMEM with 10% FBS for 30 minutes before treatment with rhTGF $\beta$ 1 (R & D systems) for 1–48 hr. Whole cell lysates were prepared in RIPA lysis buffer (Pierce) with complete Mini EDTA Protease Inhibitor and Phos-STOP (Roche) and sonication. Approximately 40 $\mu$ g of each cleared lysate were run on a 4–12% NuPAGE Bis-Tris gel and then transferred to a nitrocellulose membrane before blocking and antibody staining as above. Autoradiography bands were scanned and quantitated with ImageJ freeware. The integrated optical density of each band was normalized to GAPDH or  $\beta$ -actin and the fold change determined by dividing each normalized value by the lowest normalized sample value.

Primary antibodies used: Smad2, phospho-Smad2, phospho-Smad1/5/8, phospho-p38, Erk, phospho-Erk, phospho-SAPK/JNK, phospho-Akt (Ser 473), Snail (Cell Signaling Technology); Vimentin,  $\beta$ -actin and GAPDH (Santa Cruz Biotechnology).

### **Supplementary Material**

Refer to Web version on PubMed Central for supplementary material.

## Acknowledgments

We thank Dr. K. Symes for experimental advice and Brooke Griff for technical assistance. This work was supported by NSF (IOB 0642012; NNY), NIH (RO1 DK085300-01A1; NNY) and NCSU CCMTR (NNY, AD, MLH). AD is a Beckman Young Investigator, Cottrell Scholar, recipient of TEVA USA Scholars Grant and NSF CAREER Award.

## Reference List

- Adams DS, Robinson KR, Fukumoto T, Yuan S, Albertson RC, Yelick P, Kuo L, McSweeney M, Levin M. Early, H<sup>+</sup>-V-ATPase-dependent proton flux is necessary for consistent left-right patterning of non-mammalian vertebrates. *Development* 2006;133:1657–1671. [PubMed: 16554361]
- Bakin AV, Tomlinson AK, Bhowmick NA, Moses HL, Arteaga CL. Phosphatidylinositol 3-kinase function is required for transforming growth factor beta-mediated epithelial to mesenchymal transition and cell migration. *J Biol Chem* 2000;275:36803–36810. [PubMed: 10969078]
- Bertl E, Bartsch H, Gerhauser C. Inhibition of angiogenesis and endothelial cell functions are novel sulforaphane-mediated mechanisms in chemoprevention. *Mol Cancer Ther* 2006;5:575–585. [PubMed: 16546971]
- Bertolino P, Deckers M, Lebrin F, ten Dijke P. Transforming growth factor-beta signal transduction in angiogenesis and vascular disorders. *Chest* 2005;128:585S–590S. [PubMed: 16373850]
- Bols M, Skrydstrup T. Silicon-Tethered Reactions. *Chemical Reviews* 1995;95:1253–1277.
- Brueckner M. Heterotaxia, congenital heart disease, and primary ciliary dyskinesia. *Circulation* 2007;115:2793–2795. [PubMed: 17548739]
- Collazo A, Bronner-Fraser M, Fraser SE. Vital dye labelling of *Xenopus laevis* trunk neural crest reveals multipotency and novel pathways of migration. *Development* 1993;118:363–376. [PubMed: 7693414]
- DaCosta BS, Major C, Laping NJ, Roberts AB. SB-505124 is a selective inhibitor of transforming growth factor-beta type I receptors ALK4, ALK5, and ALK7. *Mol Pharmacol* 2004;65:744–752. [PubMed: 14978253]
- Fagotto F, Gumbiner BM. Beta-catenin localization during *Xenopus* embryogenesis: accumulation at tissue and somite boundaries. *Development* 1994;120:3667–3679. [PubMed: 7821229]
- Feng Y, Mitchison TJ, Bender A, Young DW, Tallarico JA. Multi-parameter phenotypic profiling: using cellular effects to characterize small-molecule compounds. *Nat Rev Drug Discov* 2009;8:567–578. [PubMed: 19568283]
- Green J. The animal cap assay. *Methods Mol Biol* 1999;127:1–13. [PubMed: 10503220]
- Halder SK, Beauchamp RD, Datta PK. A specific inhibitor of TGF-beta receptor kinase, SB-431542, as a potent antitumor agent for human cancers. *Neoplasia* 2005;7:509–521. [PubMed: 15967103]
- Hendrix MJ, Seftor EA, Seftor RE, Kasemeier-Kulesa J, Kulesa PM, Postovit LM. Reprogramming metastatic tumour cells with embryonic microenvironments. *Nat Rev Cancer* 2007;7:246–255. [PubMed: 17384580]
- Ho DM, Chan J, Bayliss P, Whitman M. Inhibitor-resistant type I receptors reveal specific requirements for TGF-beta signaling in vivo. *Dev Biol* 2006;295:730–742. [PubMed: 16684517]
- Inman GJ, Nicolas FJ, Callahan JF, Harling JD, Gaster LM, Reith AD, Laping NJ, Hill CS. SB-431542 is a potent and specific inhibitor of transforming growth factor-beta superfamily type I activin receptor-like kinase (ALK) receptors ALK4, ALK5, and ALK7. *Mol Pharmacol* 2002;62:65–74. [PubMed: 12065756]
- Inui M, Asashima M. A novel gene, Ami is expressed in vascular tissue in *Xenopus laevis*. *Gene Expr Patterns* 2006;6:613–619. [PubMed: 16431163]
- Jakowlew SB. Transforming growth factor-beta in cancer and metastasis. *Cancer Metastasis Rev* 2006;25:435–457. [PubMed: 16951986]
- Kamal IM. Defusing the intra-abdominal ticking bomb: intestinal malrotation in children. *CMAJ* 2000;162:1315–1317. [PubMed: 10813015]

- Kawakami T, Soma Y, Kawa Y, Ito M, Yamasaki E, Watabe H, Hosaka E, Yajima K, Ohsumi K, Mizoguchi M. Transforming growth factor beta1 regulates melanocyte proliferation and differentiation in mouse neural crest cells via stem cell factor/KIT signaling. *J Invest Dermatol* 2002;118:471–478. [PubMed: 11874486]
- Kim DS, Park SH, Park KC. Transforming growth factor-beta1 decreases melanin synthesis via delayed extracellular signal-regulated kinase activation. *Int J Biochem Cell Biol* 2004;36:1482–1491. [PubMed: 15147727]
- Kim JH, Jang YS, Eom KS, Hwang YI, Kang HR, Jang SH, Kim CH, Park YB, Lee MG, Hyun IG, Jung KS, Kim DG. Transforming growth factor beta1 induces epithelial-to-mesenchymal transition of A549 cells. *J Korean Med Sci* 2007;22:898–904. [PubMed: 17982242]
- Levin M. Left-right asymmetry in embryonic development: a comprehensive review. *Mech Dev* 2005;122:3–25. [PubMed: 15582774]
- Lipscomb K, Schmitt C, Sablyak A, Yoder JA, Nascone-Yoder N. Role for retinoid signaling in left-right asymmetric digestive organ morphogenesis. *Developmental Dynamics* 2006;235:2266–2275. [PubMed: 16786581]
- Muller J, Prather D, Nascone-Yoder NM. Left-right asymmetric morphogenesis in the *Xenopus* digestive system. *Developmental Dynamics* 2003;228:672–682. [PubMed: 14648844]
- Nieuwkoop, PD.; Faber, J. Normal Table of *Xenopus laevis* (Daudin). New York: Garland Publishing Inc; 1994.
- Ohi Y, Wright CV. Anteriorward shifting of asymmetric Xnr1 expression and contralateral communication in left-right specification in *Xenopus*. *Dev Biol* 2007;301:447–463. [PubMed: 16959238]
- Pepper MS. Transforming growth factor-beta: vasculogenesis, angiogenesis, and vessel wall integrity. *Cytokine Growth Factor Rev* 1997;8:21–43. [PubMed: 9174661]
- Reed R, Womble M, Dush M, Tull R, Bloom S, Morckel A, Devlin E, Nascone-Yoder N. The morphogenesis of the primitive gut tube is generated by Rho/ROCK/Myosin II-mediated endoderm rearrangements. *Dev Dyn* 2009;238:3111–3125. [PubMed: 19924810]
- Sive, HL.; Grainger, RM.; Harland, RM. Early Development of *Xenopus laevis*. Cold Spring Harbor, New York: Cold Spring Harbor Laboratory Press; 1998.
- ten Dijke P, Arthur HM. Extracellular control of TGFbeta signalling in vascular development and disease. *Nat Rev Mol Cell Biol* 2007;8:857–869. [PubMed: 17895899]
- ten Dijke P, Hill CS. New insights into TGF-beta-Smad signalling. *Trends Biochem Sci* 2004;29:265–273. [PubMed: 15130563]
- Tian F, DaCosta BS, Parks WT, Yoo S, Felici A, Tang B, Piek E, Wakefield LM, Roberts AB. Reduction in Smad2/3 signaling enhances tumorigenesis but suppresses metastasis of breast cancer cell lines. *Cancer Res* 2003;63:8284–8292. [PubMed: 14678987]
- Tomlinson ML, Guan P, Morris RJ, Fidock MD, Rejzek M, Garcia-Morales C, Field RA, Wheeler GN. A chemical genomic approach identifies matrix metalloproteinases as playing an essential and specific role in *Xenopus* melanophore migration. *Chem Biol* 2009;16:93–104. [PubMed: 19171309]
- Walmsley M, Ciau-Uitz A, Patient R. Adult and embryonic blood and endothelium derive from distinct precursor populations which are differentially programmed by BMP in *Xenopus*. *Development* 2002;129:5683–5695. [PubMed: 12421708]
- Whitman M, Mercola M. TGF-beta superfamily signaling and left-right asymmetry. *Sci STKE* 2001;2001:RE1. [PubMed: 11752633]
- Xu J, Lamouille S, Derynck R. TGF-beta-induced epithelial to mesenchymal transition. *Cell Res* 2009;19:156–172. [PubMed: 19153598]
- Yingling JM, Blanchard KL, Sawyer JS. Development of TGF-beta signalling inhibitors for cancer therapy. *Nat Rev Drug Discov* 2004;3:1011–1022. [PubMed: 15573100]
- Young DD, Sripada L, Deiters A. Microwave-assisted solid-supported alkyne cyclotrimerization reactions for combinatorial chemistry. *J Comb Chem* 2007;9:735–738. [PubMed: 17658900]
- Zhang YE. Non-Smad pathways in TGF-beta signaling. *Cell Res* 2009;19:128–139. [PubMed: 19114990]

Zhu L, Belmont JW, Ware SM. Genetics of human heterotaxias. *Eur J Hum Genet* 2006;14:17–25.  
[PubMed: 16251896]

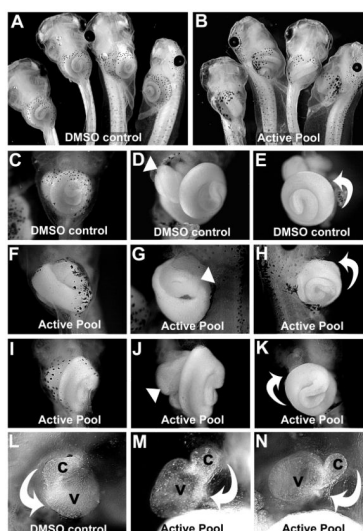


**Figure 1. A mixture of pyridine regioisomers causes heterotaxia in *Xenopus***

Embryos were treated with A) DMSO or B) 200 $\mu$ M active pool. C) Ventral view of organs in intact DMSO control tadpole. Ventral (D) and left ventral (E) views of tadpole in C with skin removed, showing the normal asymmetry (arrowhead, D) of the foregut loop, and the normal counterclockwise rotation of the intestine (curved arrow, E). F) Tadpole exposed to active pool. Ventral (G) and right ventral (H) view of tadpole in F with skin removed, showing the reversed position (arrowhead, G) of the foregut loop. The intestine is coiling in the normal direction (curved arrow, H), but is located on the opposite side of the animal. Ventral views of tadpole exposed to active pool (I-K), show normal foregut looping (arrowhead, J), but the intestine coiling in the reversed direction (i.e., clockwise; curved arrow, K). L) Ventral view of heart of DMSO control, with outflow tract (conus, c) and ventricle (v) indicated, with the normal direction of cardiac looping (curved arrow). M-N) Two examples of heterotaxin-induced reversed heart looping (curved arrows).

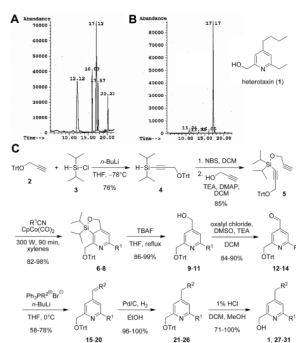


**Figure 2. Purification, identification and synthesis of heterotaxin (1)**

A) GC trace of the regioisomers in the active pool. B) Active regioisomer (1) after separation (see Supplemental Experimental Procedures), phenotypic assay, and structural assignment. C) Regioselective synthetic route towards gram quantities of heterotaxin (1) and analogs (27–31).



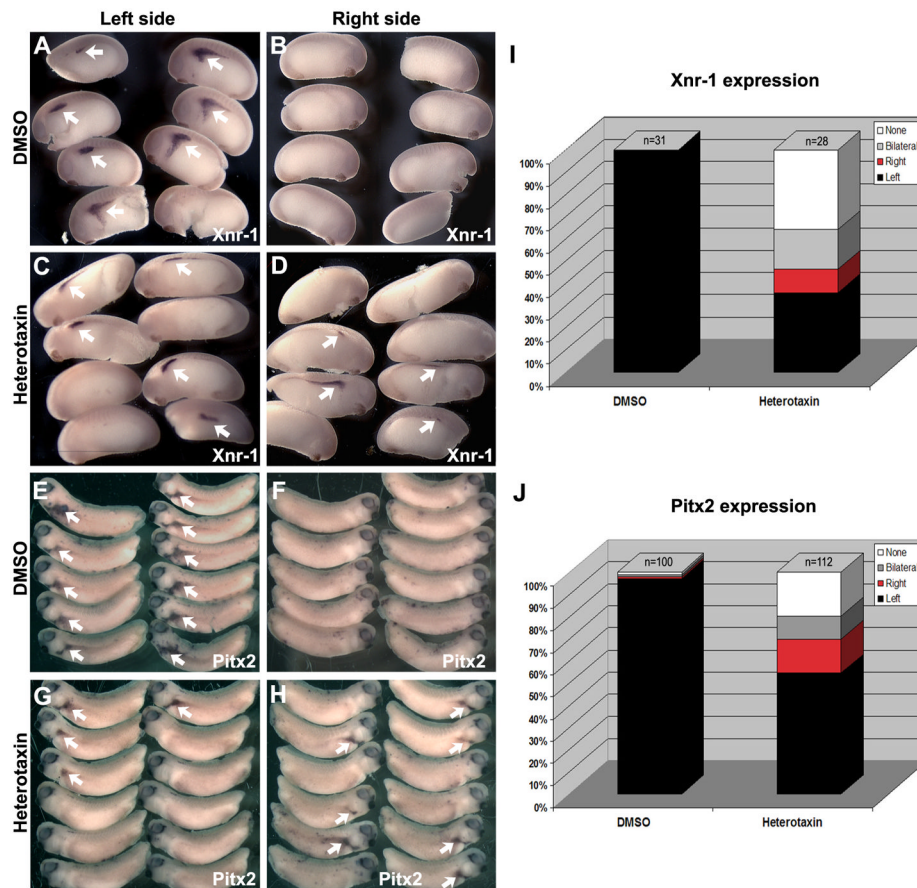


**Figure 3. Heterotaxin perturbs left-right asymmetric gene expression patterns**

AH) In situ hybridization for *nodal* (*Xnr-1*; A-D), and *Pitx2* (*XPitx2c*; E-H) genes was performed on DMSO- (A, B, E, F) and heterotaxin-treated (C, D, G, H) embryos. The expression pattern (arrows) is shown for both the left (A, C, E, G) and right (B, D, F, H) sides of the embryo (A-D, stage 23; E-H, stage 26). The frequency of embryos exhibiting left only (Left, black), right only (Right, red), bilateral (gray) or absent (None, white) expression of *nodal* (I) or *Pitx2* (J) is quantified in the bar graphs.

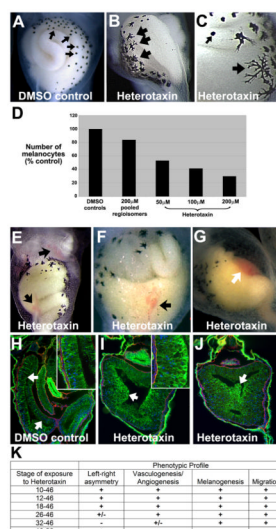


#### Figure 4. Heterotaxin perturbs melanogenesis, angiogenesis and cell rearrangements

Compared to the round melanocytes seen in DMSO controls (small arrows, A, C), heterotaxin-treated embryos (two different embryos are shown in B,C) exhibit highly dendritic pigment cells (large arrows, B-C). D) Number of abdominal melanocytes in embryos exposed to either DMSO, the active pool identified in the original pilot screen, or different concentrations of purified heterotaxin. E-G) Heterotaxin induces mild (arrows, E, F) to severe (arrow, G) defects in vasculogenesis (compare the three different examples in E-G to DMSO control in A). H-J) Immunohistochemical staining for E-cadherin (green), laminin (red) and nuclei (blue; DAPI) on frontal sections (100X) through the gut tube of embryos treated with DMSO (H, control), 100 $\mu$ M heterotaxin (I) or 200 $\mu$ M heterotaxin (J). A single-layer columnar epithelium lines the digestive tract of the DMSO tadpole (arrows, H; inset at 400X), while the cells lining the heterotaxin-treated gut are round, exhibit high levels of E-cadherin (green), and have failed to rearrange into a single layer [arrows, I (inset at 400X), J]. K) Time course studies reveal the sensitivity of each phenotype to heterotaxin exposure. “Left-right asymmetry” = reversal of heart looping, foregut looping, and/or intestinal rotation; Vasculogenesis/Angiogenesis” = hemorrhaging or enlarged blood vessels; “Melanogenesis” = decreased number and increased dendricity of melanocytes; “migration” = perturbed cell rearrangement, indicated by shortening of the primitive gut tube. “+” indicates that at least 75% of embryos exhibited the phenotype in two or more independent trials; “+/-” indicates that at least 50% of embryos exhibited the phenotype in two or more independent trials. (See Figure S1 for a similar phenotypic profile induced by a known TGF- $\beta$  inhibitor, SB-505124.)

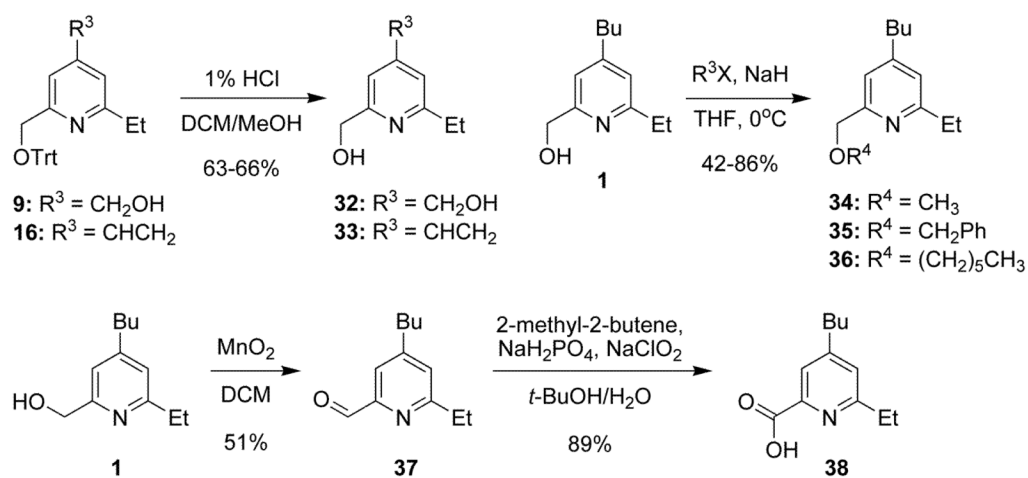


**Figure 5. Synthesis of additional heterotaxin analogs from common precursors**

See Table S1 for Structure-Activity Relationship analyses of heterotaxin analogs and Supplemental Experimental Procedures.

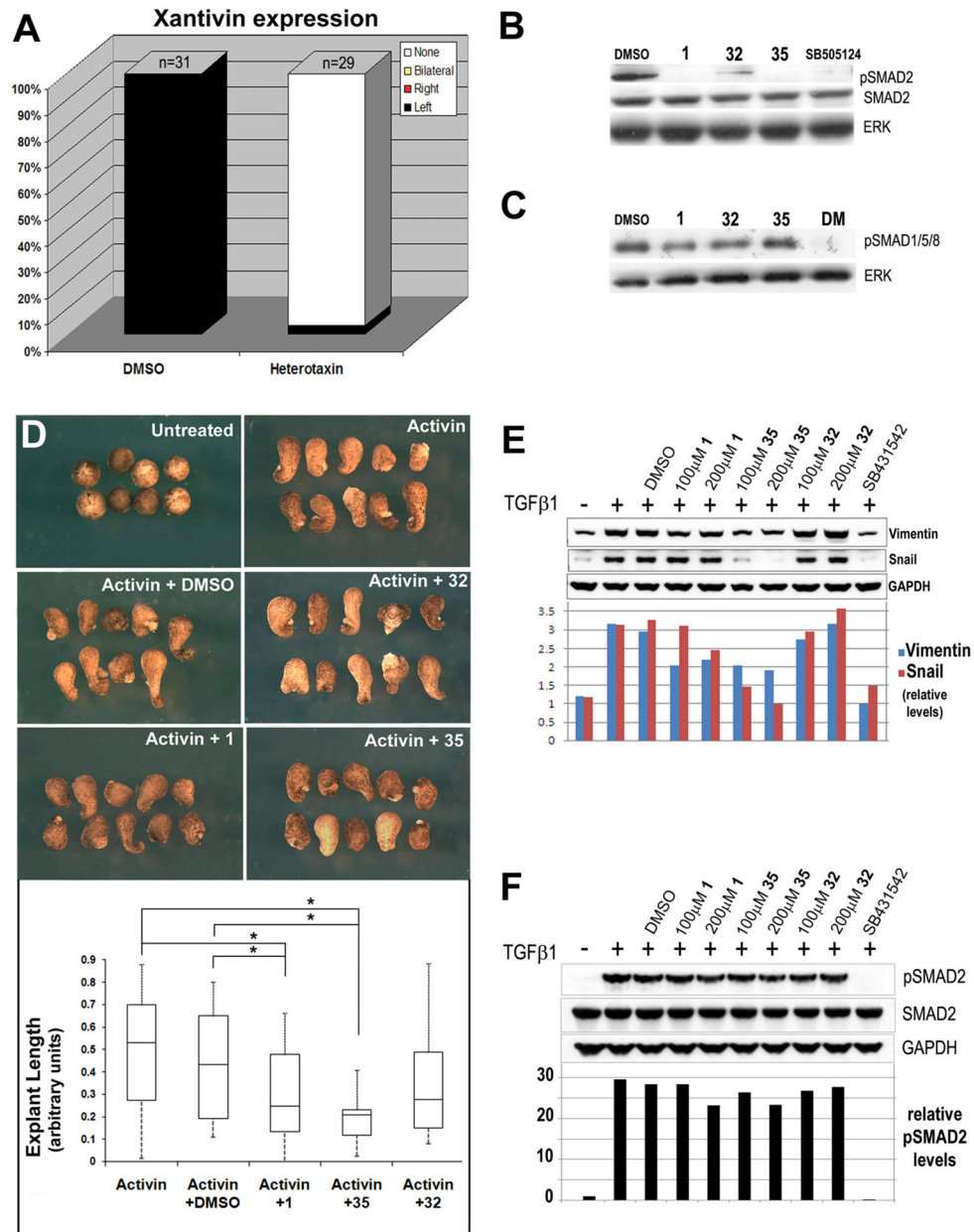


**Figure 6. Heterotaxin inhibits TGF-β signaling**

A) The frequency of embryos exhibiting left only (Left, black), right only (Right, red), bilateral (gray) or absent (None, white) expression of *Xantivin* is quantified in the bar graphs. (See Figure S2 for images of *in situ* hybridization). B) Western blotting of embryos exposed from 10 hpf for 24 hrs to DMSO, 200μM heterotaxin (1), 200μM phenotypically inactive analog (32), 80μM active analog (35) and a known *nodal* signaling inhibitor (SB-505124; 50μM). While unmodified Smad2 is detected under all conditions, phosphorylated Smad2 (pSmad2) is only detected in the presence of DMSO or the inactive heterotaxin analog 32 (albeit at reduced levels). ERK is total protein control. C) Western blotting of embryos exposed to DMSO, 1, 32, 35 and the BMP signaling inhibitor, dorsomorphin (DM; 50μM). BMP-specific Smad1/4/5 levels are unaffected by heterotaxin analogs. D) Activin-induced elongation in *Xenopus* animal cap explants is inhibited by

active heterotaxin analogs **1** and **35** but not DMSO or analog **32**. The box plot shows that activin-induced lengthening (results pooled from two identical trials) is inhibited significantly only by compounds **1** and **35**, as calculated by one-way ANOVA. \*,  $p < 0.05$ . E) Western blotting of A549 cells exposed to 10ng/ml TGF- $\beta$ 1 and DMSO, 100–200 $\mu$ M **1**, **32**, **35** or 10 $\mu$ M SB-431542 for 48 hr. TGF- $\beta$ 1-induced upregulation of Vimentin and Snail is inhibited by analogs **1** and **35** but not DMSO or analog **32**. GAPDH is total protein control. F) Western blotting of A549 cells exposed to 10ng/ml TGF- $\beta$ 1 and DMSO, 100–200 $\mu$ M **1**, **32**, **35** or 10 $\mu$ M SB-431542 for 1 hr. TGF- $\beta$ 1-induced phosphorylation of Smad2 is unaffected by heterotaxin analogs. GAPDH controls for total protein. (See Figure S2 for effect of **1** on non-Smad-dependent TGF- $\beta$  signaling via PI3K/Akt.)

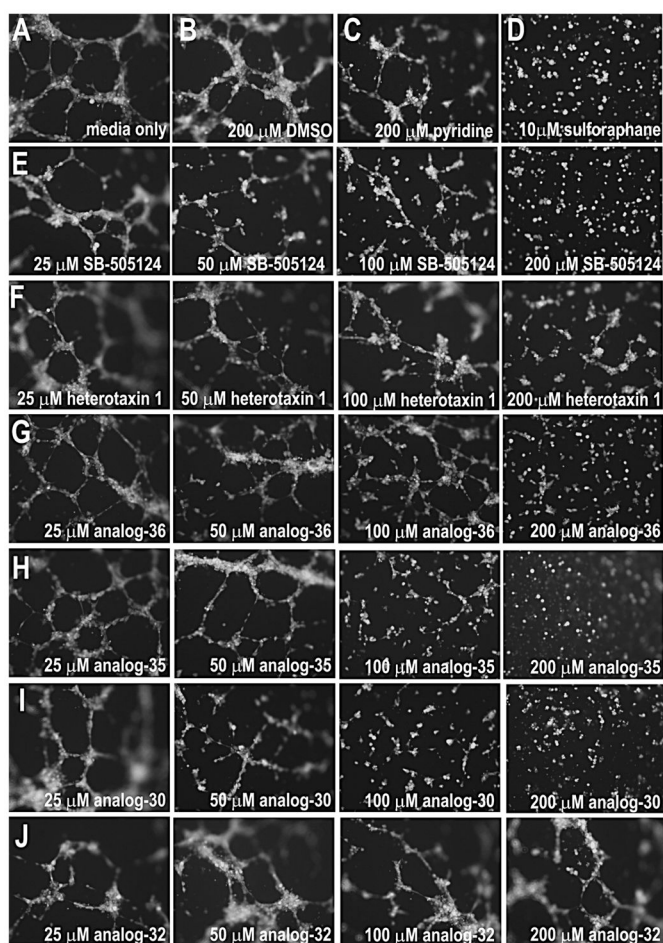


### Figure 7. Heterotaxin inhibits angiogenesis in human cells

Human umbilical vein endothelial cells (HUVECs) form tubes when cultured in the presence of media alone (A), DMSO (B), unsubstituted pyridine (C), or the inactive heterotaxin analog **32** (J). In contrast, HUVECs cultured in the presence of a known anti-angiogenic agent (D, sulforaphane; Bertl et al., 2006) are unable to form tubes. Although the original heterotaxin molecule **1** (F) exhibits only very mild anti-angiogenic effects in this assay (at 6 hr), the other active heterotaxin analogs **36** (G), **35** (H) and **30** (I) have obvious concentration-dependent anti-angiogenic properties comparable to a known TGF- $\beta$  signaling inhibitor (E, SB-505124). Cells were stained with Calcein AM to confirm viability. (See Figure S3 for effect of analog **30** on tumor cell growth.)